Volume 1 | Number 1 | Jan 2013 | Pages 1–100

Nanoscale

www.rsc.org/nanoscale

ROYAL SOCIETY OF CHEMISTRY

ROYAL SOCIETY OF CHEMISTRY

www.rsc.org/nanoscale

Nanoscale

PAPER

Nanoscale Accepted Manuscript

808 nm Driven Nd³⁺-Sensitized Upconversion Nanostructures for Photodynamic Therapy and Simultaneous Fluorescence Imaging

Dan Wang,[a,b,+] **Bin Xue,**[a,b,+] **Xianggui Kong,*[a] Langping Tu,**[a,b] **Xiaomin Liu,**[a] **Youlin Zhang,**[a] **Yulei Chang,**[a] **Yongshi Luo,**[a] **Huiying Zhao**[c] **and Hong Zhang***[d]

Abstract

In vivo biological application of upconversion nanoparticles (UCNPs) prefers excitation of 700-850 nm, instead of 980 nm, due to the absorption of water. Recently approach in constructing robust Nd³⁺ doped
10 UCNPs subject to 808 nm excitation relies on a thick Nd³⁺ sensitized shell. However, for the very important and popular Förster resonance energy transfer (FRET)-based applications, such as photodynamic therapy (PDT) or switchable biosensor, this structure has its restriction resulting in a poor energy transfer. We have in this work designed the NaYF₄:Yb/Ho@NaYF₄:Nd@NaYF₄ core-shell-shell nanostructure. It is proved that this optimal structure balances the robustness of the upconversion
15 emission and the FRET efficiency for FRET-based bio-application. A proof of the concept was demonstrated for photodynamic therapy and simultaneous fluorescence imaging of Hela cell triggered by 808 nm light, where low heating and high PDT efficacy were reached.

1. Introduction

Lanthanide-doped upconversion nanoparticals (UCNPs) have
20 been various elaborately designed[1-6] due to they provide enuomous potential applications in bioimaging, drug delivery, sensors, data storage,[7-10] and in particular distance-dependent Förster resonance energy transfer (FRET, also referred to as luminescence resonance energy transfer (LRET))-based
25 applications such as molecular photo-switch, biosensing, and photodynamic therapy (PDT).[11-13] For in vivo bioapplication, the upconversion nanoparticles excitable by 980 nm have till now been the focus since this excitation wavelength falls in so-call "optical window" of tissue and the biological environment is
30 hardly excited, leading to a high quality, as well as relatively deep depth, of the imaging. However, 980 nm is at the rising edge of the absorption of tissue (although much lower than visible light) and can still be absorbed by water. In the consequent overheating effects limits the power of the excitation light.[7]
35 Various efforts have been made to improve the performance of the upconversion nanomaterials in this aspect. Recently, Nd³⁺-sensitized UCNPs with 800 nm laser excitation were reported. Han et al. found that triply doping Nd³⁺, Yb³⁺, and activator in NaYF₄ could get upconversion emission under 800 nm
40 excitation.[8] Yb³⁺ions act as a bridge to transfer the energy from the Nd³⁺ions to the activators. For the triple doping in NaYF₄, due to quenching effects between the activators and Nd³⁺ ions, the upconversion emission was very weak. Several groups spatially separated activators from Nd³⁺ ions via core-shell structure to
45 acquire high efficient luminescence under 800 nm excitation.[9-12] Although the upconversion luminescence (UCL) fulfilled by a thick Nd³⁺ sensitizing shell could be used for bioimaging, this

structure is not appropriate for FRET-based applications, such as homogeneous bioassays, biosensing and PDT, which are in
50 general based on energy transfer mechanism. For example, for UCNPs –based PDT, the luminescence activators inside the nanoparticles (as the energy donors) transfer the excitation energy to the acceptors *i. e.* photosensitizing molecules (photosensitizers) to generate cytotoxic singlet oxygen (¹O₂, type II) to kill cancer
55 cells. The energy transfer rate depends strongly on the distance between the donors (activators) and the acceptors (photosensitizers).[13]Though spatially separating activators and Nd³⁺ ions could get higher UCL efficiency, this Nd³⁺ sensitizer layer may lead long distance between activators and
60 photosensitizers, which is not favorable for FRET process of PDT. Moreover, in contrast to bioimaging, PDT requires higher upconversion efficiency because it performs under irradiation of lower power density. Since spatial separation of activators from Nd³⁺ ions is essential for high upconversion luminescence
65 efficiency, the challenge for FRET-based biological applications is how to achieve a high UCL efficiency and an effective FRET under ~800 nm excitation.

In this work we overcame the difficulty by balancing high UCL and high efficiency of FRET via constructing a novel
70 NaYF₄:Yb/Ho@NaYF₄:Nd@NaYF₄ core-shell-shell structure. Proof of concept of its application on FRET-based PDT application is demonstrated. The outermost inert layer was to improve the UCL to compensate UCL deleterious effect due to the decreased Nd³⁺-sensitized layer. By using this novel
75 nanostructure, PDT without overheating effects and simultaneous UCL imaging under 808 nm excitation was realized.

2. Experimental section

2.1 Materials

NdCl$_3$ 6H$_2$O (99.9%), HoCl$_3$ 6H$_2$O (99.9%), YbCl$_3$ 6H$_2$O (99.9%), YCl$_3$ 6H$_2$O (99.9%), Oleic Acid (90%) (OA), 1-octadecene (90%) (ODE), Y(CF$_3$COO)$_3$, Yb(CF$_3$COO)$_3$, CF$_3$COONa, Rose Bengal, Hexanoic Acid, Poly(allylamine) (PAAM), dimethyl formamide(DMF), mPEG-succinimidyl carbonate(MPEG-SC), 1-ethyl-3-(3-dimethylaminopropy) carbodiimide (EDC), N-hydroxy-succinimide (NHS), 1,3-diphenylisobenzofuran (DPBF) were all purchased from Sigma-Aldrich. Nd(CF$_3$COO)$_3$, Ho(CF$_3$COO)$_3$ were made from Nd$_2$O$_3$ and Ho$_2$O$_3$ in excess CF$_3$COOH and evaporate CF$_3$COOH. 4% paraformaldehyde, 4',6-diamidino-2-phenylindole (DAPI) were purphased from Beyotime Institute of Biotechnology; NaOH, NH$_4$F and dimethyl formamide were purchased from Beijing Chemical Works. All other chemical reagents were of analytical grade and were used directly without further purification.

2.2 Synthesis of β-NaYF$_4$: Yb/Ho(8/1%)@NaYF$_4$:Nd(20%)@ NaYF$_4$ core-shell-shell nanopaticals :

β-NaYF$_4$: Yb/Ho(8/1%)@NaYF$_4$:Nd(20%)@ NaYF$_4$ core-shell-shell nanopaticals were synthesized based on a previously reported procedure.[14] YbCl$_3$ 6H$_2$O (99.9%) 0.04 mmol, YCl$_3$ 6H$_2$O (99.9%) 0.445 mmol and HoCl$_3$.6H$_2$O(99.9%) 0.005 mmol were dissolved in 3 mL OA, 7.5 mL ODE, and the mixture was heated 150℃ under argon protection. NH$_4$F (2mmol), NaOH (1.25mmol) were dissolved in 5mL methanol and added to three neck flask. Afterwards, the solution was heated to 70°C to remove methanol and subsequently heated to 300 ^{o}C for 1 hour. After that, 1 mmol NaYF$_4$: Nd (20%) active shell in octadecene was injected into reaction mixture and ripened for 10 min, and then another NaYF$_4$ inert shell (1 mmol) materials was added and ripened for 10 min. Finally, the solution was cooled down to room temperature and precipitated ethanol, collected by centrifugation and dispersed in 6 mL hexane.

Synthesis of different thickness of active shell of β-NaYF$_4$:Yb/Ho(8/1%) @ NaYF$_4$:Nd(20%) @ NaYF$_4$ core-shell-shell nanopaticals : the synthesis was carried out exactly as outlined for β-NaYF$_4$:Yb/Ho(8/1%) @ NaYF$_4$:Nd (20%) @ NaYF$_4$ nanoparticals mentioned above, except that the ratio of injected small sacrifice nanoparticals (SNPs) α-NaYF4:Nd(20%) was 0.05mmol, 0.1mmol, 0.3 mmol, 0.5 mmol, respectively. After that, 0.1 mmol, 0.15 mmol, 0.17 mmol, 0.2 mmol inert NaYF$_4$ shell was injected, ripening for 5 minutes.

2.3 Synthesis of Amino-Functionalized UCNPs:

To obtain amio-functionalized UCNPs, a ligand exchange approach was adopted using PAAm to transform the hydrophobic UCNPs into hydrophilic ones. 50μL (20wt%) PAAm was diluted with 4mL CH$_3$CH$_2$OH, then UCNPs (200μL, 2mg/mL) was added to PAAm solution, ultrasound for 2minutes, and stirred for 24 hours at room temperature. After centrifugation for two times, the products were dispersed in water for further functionalization.

2.4 Covalent conjugation of UCNPs with Rose Bengal

To compare the ^{1}O$_2$ generation from four different thickness of active-shell UCNPs, covalent conjugation of UCNPs with Rose Bengal was similar with Liu et al.[15] with a little modification. The Rose Bengal hexanoic acid (RB) was obtained according the reference.[16] In order to covalently RB to amino-functionalized UCNPs, 4 mL of dimethyl formamide solution containing 0.2 mg of RB, 2 mg of EDC, and 0.5 mg of NHS was incubated for 30 min, and then 20 mg of amino-functionalized UCNPs was added into solution and reacted for 16 h. And then UCNPs-RB centrifuged with deionized water for three times and rediperse in PBS. From the RB absorption spectrum, about 38 RB molecules were covalent on one nanoparticles.

2.5 Singlet oxygen determination

DPBF was used to determine the singlet oxygen generation.[17] In a typical DPBF experiment, 10 μL of a DPBF/ethanol solution (8 mM) was added to 2 mL of RB-UCNPs solution. And then the whole solution was irradiated by 808 nm laser light at the same power density (0.67 W/cm^2), and the absorption of DPBF at 417 nm was collected at every 2 minutes. The procedure was the same for the other different active shell thickness UCNPs-RB detection ^{1}O$_2$ experiments.

2.6 Number of coupling RB molecules

The number of coupling RB amounts was calculated from the RB absorption spectrum. In a typical experiment, 10 μL, 20ul, 30 μL, 40 μL, 50 μL, 60 μL RB-HA solution (10 mg/mL), EDC 2mg, NHS 0.4 mg were added to 0.5 mL UCNPs (10 mg/mL) solution, respectively, stirred for 16h at room temperature. Then they were washed with DMF for three times for UV-Vis absorption.

2.7 UCNPs were covalent with FA and PEG-SC

In order to specific targeting to cancer cells, FA was introduced covalently to UCNPs-RB. In a typical experiment, 2 mg of FA, 1 mg PEG-SC, 2 mg of EDC, 0.5 mg NHS and 10 mg of UCNPs-RB were added in 5 mL DMF, and stirred for 12 h, and then centrifuged, dispersed in PBS.

2.8 Comparing the overheating effects of 808 nm laser and 980 nm laser

In order to further verify the overheating effects induced by 808 nm and 980 nm laser, Hela cells were seeded into two 96-well at concentration of 10^4 cells/well (100μL) and then incubated for 24 hours at 37 ^{o}C under 5% CO$_2$. Then the cells were exposed to 808 nm laser and 980 nm laser at different power densities of 0.67 W/cm^2, 1.15 W/cm^2 and 1.62 W/cm^2, respectively. And then the cells were incubated for 24 h. Then the MTT solution (5mg/mL, 20μL) was added and incubated 4h, then, replaced with 150μL DMSO into each well. The absorbance in each well was measured at 492 nm. Cell viability was calculated using the following formula: Cell viability was calculated using the following formula: Cell viability = (mean absorbance of test wells − mean absorbance of medium control wells) / (mean absorbance of untreated wells − mean absorbance of medium control well) $\times 100\%$.
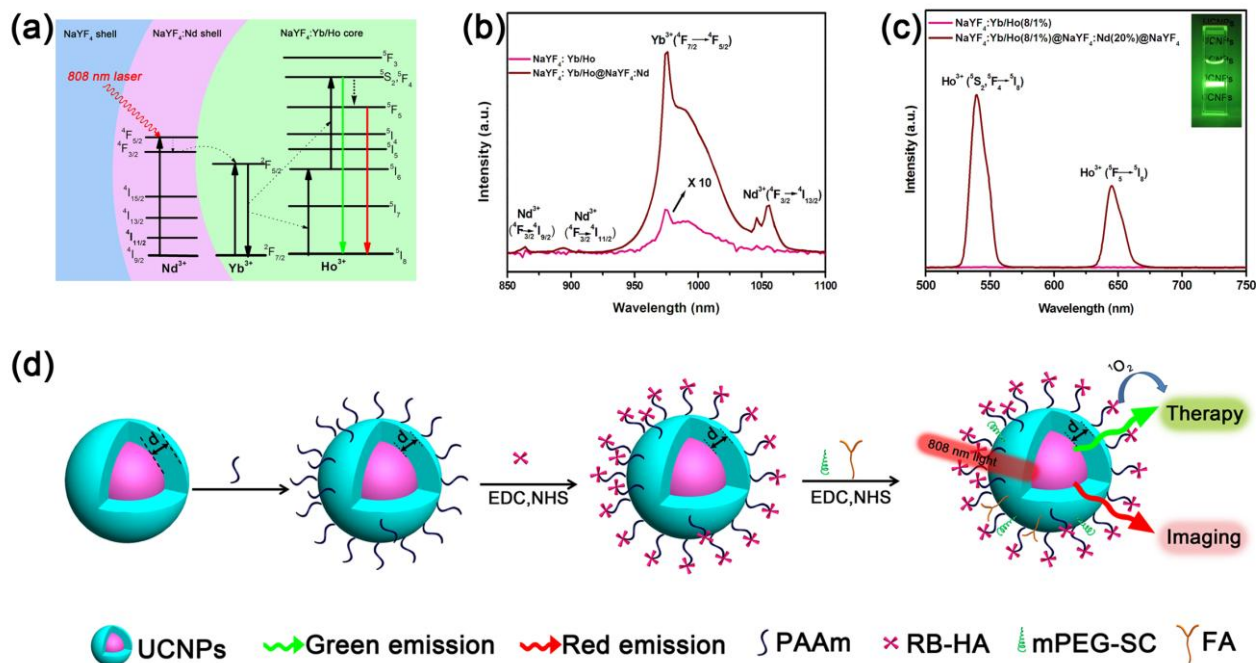
Fig. 1 (a) Upconversion mechanism of nanostructure with excitation of 808 nm laser. (b) NIR emission spectra of NaYF₄:Yb/Ho (8/1%) nanoparticles and NaYF₄:Yb/Ho(8/1%)@NaYF₄:Nd(20%) nanoparticles. (c)Room-temperature upconversion emission spectra ofNaYF₄: Yb/Ho(8/1%) nanoparticles and NaYF₄: Yb/Ho(8/1%)@NaYF₄:Nd (20%)@ NaYF₄ nanoparticles. (d) The construction and operating principle of the nanoplatform for photodynamic therapy and imaging.

2.9 MTT assays for cytotoxicity

Cytotoxity of UCNPs-RB was evaluated by Hela cancer cells. The cells were seeded in 96-well plates (1×10^4 cells/well). After 24 h cultivation, 100 μL UCNPs-RB of different concentrations (0, 50, 100, 150, 200, 400, 600μg/mL) were added into the wells and incubated for 48 h. Then MTT solution (20μL, 5 mg/mL) was added into each well. After 4 h incubation at 37°C, the MTT solution was replaced with 150μL DMSO into each well. The absorbance in each well was measured at 492 nm.

2.10 In vitro cancer cell imaging

In our experiment, Hela cells and A549 cells were seeded into three culture dishes at concentration of 10^4 cells/ per culture dish (100μL) and incubated for 24 hours at 37°C under 5% CO_2. Then, Hela cells were cultured in RPMI-1640 medium incubated with FA and PEG-SC functionalized UCNPs-RB (200μg/mL, 100μL) were used as positive group. Hela cancer cells were cultured in folate-free RPMI medium incubated with UCNPs-RB (200μg/mL, 100μL) was used as control group.

In another control group, we used A549 cells incubated with FA and PEG-SC functionalized UCNPs-RB at same concentration. All the cells were incubated 4 h, and washed with phosphate buffered saline (PBS) to fully remove excess UCNPs-RB nanoconstructs. Fixing cells by added paraformaldehyde (4 wt%, 1 mL) in each culture dish for 10 minutes. Cell nuclei were stained with DAPI (1mL/ per culture dish) for 10 minutes. After washing five times with PBS, the cells were imaged by a laser confocal microscope (Nikon Confocal Microscope C2/C2si). UCL imaging of UCNPs-RB was performed by using confocal microscope equipped with an external 808 nm laser.

2.11 In vitro PDT

100μL Hela cells were seeded into 96-well at the concentration of 10^4 cells/well, and then incubated for 24 hours at 37°C under 5% CO_2. After that, the cells were incubated with FA and PEG-SC functionalized UCNPs-RB of different concentrations (0, 50, 100, 150, 200, 400, 600μg/mL) and incubated for another 24 h, and then the cells were washed with PBS to remove unbounded UCNPs-RB nanoconstructs. After irradiated for 10 min by 808 nm laser at a power density of 0.67W/cm², the cells were incubated for 4 h at 37°C, incubated for 2h, then removed medium and washed by PBS, the MTT solution (5mg/mL, 20μL) was added and incubated for 4 h, then replaced with 150μL DMSO into each well. The absorbance in each well was measured at 492 nm.

2.12 General sample characterizations

The transmission electron microscopy (TEM) measurement was carried out on a JEM-2100F electron microsocopy operating at 200 KV. X-ray diffraction (XRD) measurements were performed with a Rigaku D/max-2000 diffractometer using Cu Ka radiation (λ=1.5406 Å).Ultraviolet-visible (UV) absorption was recorded by UV-3101 spectrophotometer. Upconversion spectra were recorded at room temperature with Maya 2000 visible spectrometer (Ocean optics) with the excitation source adapted to 808 nm fiber coupled diode lasers. NIR emission spectra were obtained with TRIAX 550 spectrometer under excitation of 808 nm diode lasers. Luminescence digital photographs were taken with SONY digital camera. The cells were imaged in bright field and fluorescence field by using NIKON confocal microscope C2-SI equipped with 808 nm NIR laser.

3. Results and discussion

The designed core-shell-shell nanostructure with excitation of 808 nm laser is illustrated in Figure 1a. These hexagonal-phase NaYF₄:Yb/Ho@NaYF₄:Nd@NaYF₄core-shell-shell nanoparticles were synthesized according to a previous report with certain modification (Supplementary experimental section and Fig.S1,

S2).[14] To enhance the upconversion emission, $NaYF_4$ inert layer was coated on the outermost layer to avoid the excitation energy loss of the nanosystem. Ho^{3+} ions (activator) were embedded in the core and Nd^{3+} ions in the shell layer, to harvest 808 nm light, respectively. Under excitation of 808 nm light, the UCL was achieved by an initial energy transfer from Nd^{3+} to Yb^{3+}. Due to

power density in a small extent will result in big enhancement of UCL (Fig. S3). Coating inert shell helps transferring more energy from Nd^{3+} ions (especially at the surface) to Yb^{3+} ions, resulting in increasing more excitation of Yb^{3+}, which is equivalent to the increase of excitation power, enhance UCL quite effectively. It is observed that coating a 1.5 nm thick $NaYF_4$ inert layer is
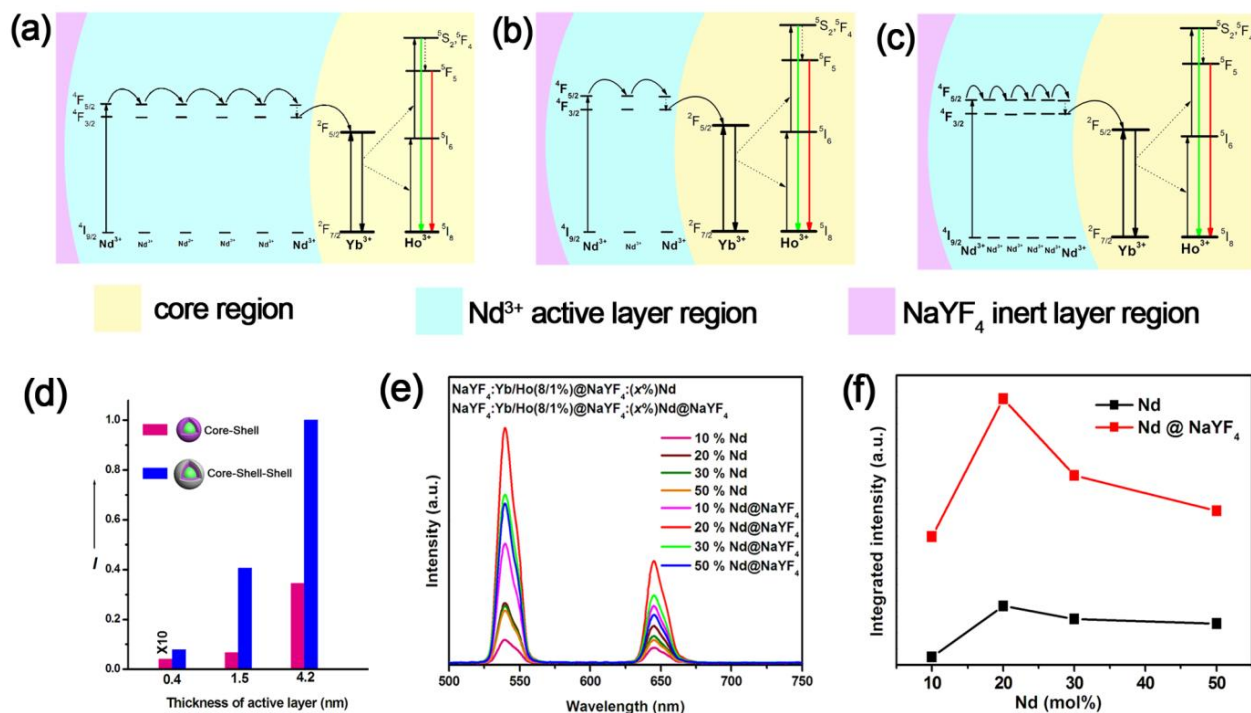

Fig. 2 Proposed energy transfer mechanisms of nanoparticle with (a) thick active layer, (b) thin active layer, (c) high concentration of Nd^{3+} in the thin active layer. (d) UC emission intensity comparison of $NaYF_4:Yb/Ho(8/1\%)$ @ $NaYF_4:Nd(20\%)$ nanoparticles of different thickness of active layer(0.4 nm,1.5 nm, 4.2 nm), without and with a thin inert layer protection ($NaYF_4$) in cyclohexane solution (20mg/ml). (e)Room-temperature upconversion emission spectra of $NaYF_4:Yb/Ho(8/1\%)@NaYF_4:Nd(x\%)$ (x=10, 20, 30, 50) and $NaYF_4: Yb/Ho(8/1\%)@NaYF_4:xNd@ NaYF_4$ (x=10, 20, 30, 50) under 808 nm excitation. (20mg/ml) .(f) integrated intensity of the upconversion emission as a function of Nd^{3+}. The spectra were recorded under excitation by an 808 nm continuous-wave laser.

the highly efficient energy transfer from Nd^{3+} to Yb^{3+}, the emission of Yb^{3+} ions at 975 nm ($^2F_{5/2} \rightarrow {}^2F_{7/2}$) was enhanced with 47.4 times by the shell under 808 nm excitation (Figure 1b). Consequently, the Yb^{3+} ions transferred the energy to Ho^{3+} ions under the framework of classical energy transfer upconversion (ETU). Here, the bright green UC emission (Figure 1c) of 540 nm ($^5S_2/^5F_4 \rightarrow {}^5I_8$) and the red UC emission of 650 nm ($^5F_5 \rightarrow {}^5I_8$) of Ho^{3+} can be observed and used for PDT and bio-imaging, respectively (Figure 1d). It was noted that, a weak emission of Yb^{3+} was observed when the bare core of $NaYF_4: Yb/Ho$ nanoparticles were excited under 808 nm laser (Figure 1b). Since Ho^{3+} ions ($^5I_8 \rightarrow {}^5I_4$) have weak absorption near 808 nm,[22] which results in the populating the $^5I_4$ under 808 nm excitation. After following multiphonon relaxation from $^5I_4 \rightarrow {}^5I_5$, Ho^{3+} ions may transfer the excitation energy to Yb^{3+} ions, which gives rise to the weak emission of Yb^{3+}.

When the nanostructure used for PDT and other FRET-based applications, the UCL should be as high as possible. $NaYF_4$ inert layer effectively enhance UCL through suppressing the surface quenching effects.[18] As is well known, UCL intensity, I, for two photon process, is nearly proportional to the square of absorbed excitation power density I_{ex}. Therefore, increasing excitation

efficiently to enhance the UCL (Fig. S4), UCL intensity increase is close to saturation for thicker inert layer.

More importantly, we found that inert shell could enhance UCL more effectively when the thickness of active Nd^{3+} layer became thin. Fig. 2d shows that the UCL was enhanced 15.1, 6.08, 2.9 times, respectively, when the thickness of active layer was 0.5 nm, 1.5 nm, 4.2 nm. The results indicate that the enhance factor of UCL was larger when active layer was thinner. This can be explained by the fact that Nd^{3+} ions in the thicker active layer needs more transfer steps from Nd^{3+} ions on outmost surface to Yb^{3+} ions in core (Fig. 2a, 2b), which will lower the enhanced ability of inert layer. All these can be further confirmed by the fact that the enhance ability of inert layer decreased with the concentration of Nd^{3+} ions. Fig. 2e-2f show the enhance factor decreased from 4.01 to 2.53 when the concentration of Nd^{3+} ions increased from 10 % to 50 % (the active layer was ~5nm). This is because that when the concentration of Nd^{3+} ions increased, the separation between Nd^{3+} was shortened. So when keep the constant of shell thickness, the increased excitation energy by inert layer also need more transfer steps to inner core (Fig. 2b, 2c). This could be further confirmed by the bigger enhance factor of NIR stokes emission of Yb^{3+} (Fig. S5, Fig. S6), when the transfer

steps were less. So when the transfer steps are less, inert layer could more effectively enhance UCL intensity when the transfer steps.

This effect is very useful because, when UCNPs used as donors for PDT or other FRET-based applications, the active layer should be as thin as possible to increase energy transfer efficiency between the activators and outmost acceptors. For the case of thinner active shell, the UCL will be weaker owing to the relatively less light absorption from smaller amounts of Nd^{3+} ions in thin sensitizer layer. Fortunately, the thin inert shell (1.5nm) could significantly strengthen the UCL in this case. The UCL of nanostructures with overall thickness 3 nm (1.5nm active layer +1.5 nm inert layer) even higher than nanostructures with only active layer of 4.2 nm (Fig. 2d). This indicates that our designed nanostructure (active layer + inert layer) will get higher UCL with thinner thickness of shell than only active layer, which is favorable for FRET applications, especially for PDT.

To acquire highly efficient UCL of UCNPs, the arrangement of Nd^{3+} as sensitizers was also optimally prepared. The maximal intensity was reached at the concentration of ~20 % Nd^{3+} (Fig. 2e, 2f). The UCL intensity declined at a higher concentration of Nd^{3+}, which may be ascribed to the more seriously cross-relaxation occurring among Nd^{3+} ions. Moreover, higher concentration of Nd^{3+} ions also resulted in more seriously quenched of quenching effects to Ho^{3+} (Fig.S7), which also limits the doped concentration of Nd^{3+} ions.
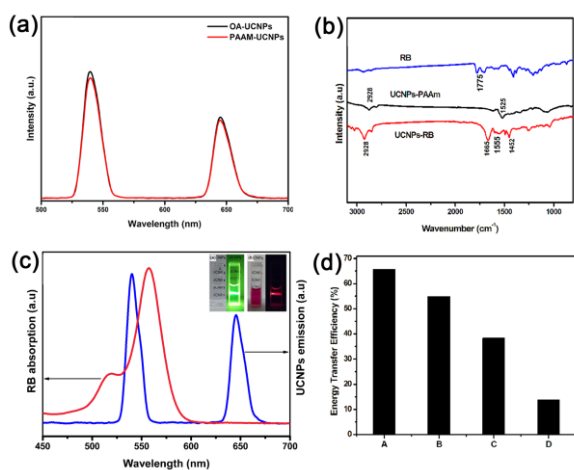

Fig. 3 (a) Upconversion spectra of UCNPs before and after phase transfer. (b) Infrared absorption spectra of free RB-HA, PAAM-UCNPs and RB-UCNPs. (c) Spectral overlap between the donors UCNPs emission spectrum (blue line) and absorption spectrum of the acceptor RB (red line). (d) Energy transfer efficiency of the four UCNPs-RB samples A-D (A for 0.4 nm, B for 1.5 nm, C for 2.6 nm and D for 4.2 nm active layer in thickness, respectively).

Till now, we have got a highly efficient core-shell-shell structure for UCL with excitation of 808 nm, but the FRET efficiency should also be concerned when UCNPs is used for FRET-based biological applications, such as PDT. For PDT, the yield of $^1O_2$ generation is determined by two factors: excitation intensity on organic photosensitizers and FRET efficiency from UCNPs to organic photosensitizers. But the shell thickness has two opposing effects on the above two factors. Thicker shell facilitates UCL resulting in the more effective excitation of photosensitizer, e.g. Rose Bengal (RB). But, on the other hand, it

reduces the FRET efficiency due to the increase of the transfer distance between the luminescent Ho^{3+} ions in core and RB. Therefore, a trade-off of the two conflicting requirements has to be reached for the optimal generation of $^1O_2$. For this reason, we synthesized different samples with various thickness of active-shell to determine a critical thickness. All the samples have the same ions concentration, i.e. 8 mol% Yb^{3+} and 1 mol% Ho^{3+} in the core and 20 mol% Nd^{3+} in the active layer. Samples A, B, C, D have nearly the same size of core and same thickness of inert layer, but different thickness of active layer, such as A (0.4 nm
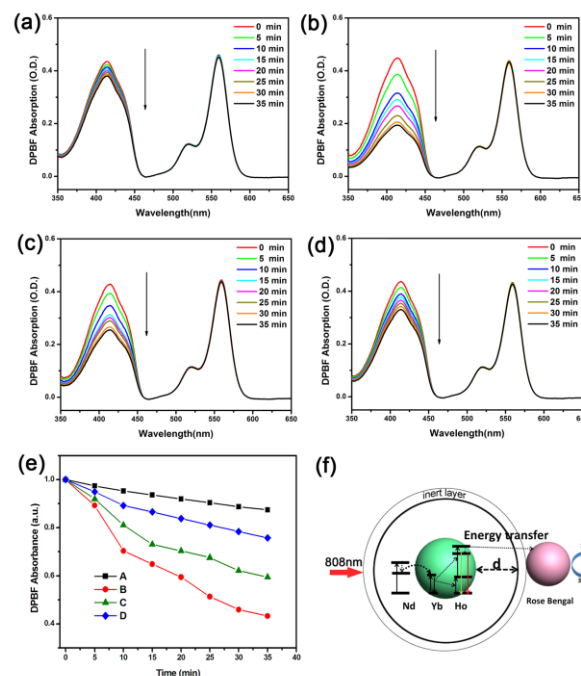

Fig. 4 Absorption spectra of DPBF (10 μL, 8 mM) incubated with NaYF₄:Yb/Ho(8/1%)@NaYF₄:Nd (20%) @NaYF₄ with different thickness of NaYF₄:Nd(20%) active-shell nanoparticles under 808 nm irradiation for every 5 minutes:(a) sample A (0.4 nm);(b) sample B (1.6 nm);(c) sample C (2.5 nm);(d) sample D (4.2 nm). (e) Absorbance at 410 nm of DPBF in ethanol solutions of A-D as a function of irradiation time. (f) Illustration diagram of changing the thickness of NaYF₄:Nd(20%) active-layer of nanoparticles for production of $^1O_2$.

active layer, Fig. S8), B (1 nm active layer, Fig. S9), C (2.5 nm active layer, Fig. S10), D (4.2 nm active layer, Fig. S11). The UCL increases in intensity with the increase of active layer due to more light harvested by more Nd^{3+} ions (Fig. S12).

To acquire a high FRET efficiency, UCNPs need be covalently coupled with organic photosensitizers RB. Similar to our previous reports.[15] We functionalized the nanoparticles and depicted the process in (Fig. 1d). We firstly transferred the UCNPs to aqueous solution without significant change of the UCL (Fig. 3a). Afterwards, the water soluble amine-functionalized UCNPs were covalent linked with RB through traditional 1-ethyl-3-(3-dimethylaminopropyl) carbodiimide hydrochloride (EDC) coupling reaction (Supplementary experimental section). The formed amide bonds could be confirmed by infrared absorption spectra (Fig. 3b)). The C=O at 1775cm⁻¹ was confirmed stretching vibration mode of the carboxyl group of RB-HA (Fig.3b,top); After PAAm phase

transfer, there was a peak at 1525cm^{-1}, which attributed to N-H stretching vibration modes (Fig. 3b,middle); Finally, conjugating with RB, the peak at 1525 cm^{-1} disappeared and two new peaks around 1665cm^{-1} and 1452 cm^{-1}appeared, which suggested C=O
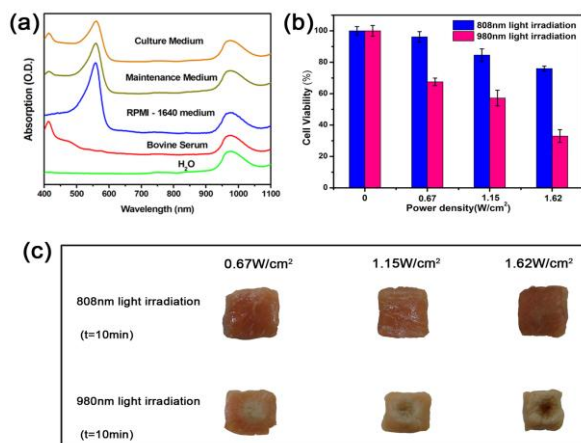5 bending vibration and C-N stretching vibration modes. The peak

Fig. 5 (a) Absorption spectra of water, bovine serum, RPMI-1640 medium cell culture maintenance medium (1% bovine serum and 99% RPMI-1640), cell culture medium (2% bovine serum and 98% RPMI-1640). (b) Heating effects of 808 nm and 980 nm lasers evaluated by viability of Hela cancer cells. (c) Morphology changes of pork tissues after continuously irradiated by 808 nm laser and 980 nm laser for ten minutes at same power density.

at 1555cm^{-1} was ascribed to the N-H bending vibration mode (Fig. 3b, bottom). All the absorptions at 2928 cm^{-1} indicate oleic acid C-H stretching vibration modes. After covalently coupling with RB, the green emission of UCNPs quenched significantly (Fig. 3c
10 top right corner), indicating the present of FRET from UCNPs to RB due to the spectral overlap of RB and UCNPs (Fig. 3c). The FRET efficiency can be measured experimentally and is commonly defined as[19]: E = (I$_0$ – I$_1$) / I$_0$, where I$_0$ and I$_1$ are green emission intensities of UCNPs before and after covalent linking
15 with RB, respectively. The FRET efficiency gradually decreased from sample A (65.7%) to D (13.8%) with increasing thickness of active layer owing to longer distance between UCNPs and RB molecules as we anticipated (Fig. 3d and Fig. S13).

20 The results above certainly demonstrate that the active shell has two opposing effects on UCL and FRET efficiency, therefore a critical thickness exists for the highest yield of $^1O_2$. Fig. 4f show schematic design of different thickness of NaYF$_4$: Nd (20%) active-shell covalent Rose Bengal for production of $^1O_2$.The
25 critical thickness of the active layer could be determined through the final product of $^1O_2$ from UCNPs-RB conjugation with 808 nm irradiation. We used traditionally chemical probe of 1, 3-diphenylisobenzofuran (DPBF) [17] to identify the generation of $^1O_2$. The decrease in absorption (~417 nm) of DPBF is
30 proportional to the production of $^1O_2$. Fig. 4a-4d show the absorption spectra of four UCNPs-RB samples (2 mg/mL) incubated with DPBF (10 µ L, 8 m M) under irradiation of 808

nm for every 5 minutes. Absorption decrease at 417 nm was observed for all the samples, showing the increase of $^1O_2$.
35 Obviously, sample B with the shell thickness of 1.5 nm is the best for $^1O_2$ production, followed by C, D and A (Fig. 4e). Although sample B neither show strongest upconversion emission nor the highest energy transfer efficiency, the biggest production of $^1O_2$ was sample B, which properly balance the UCL intensity and
40 FRET efficiency.

Before applying these UCNPs to biological applications, the heating effect should be evaluated of 808 nm laser to find the safe power density for biological application. For UCNPs-based PDT, the big problem is that the excitation light of 980 nm is at the
45 rising edge of the absorption of tissue (although much lower than visible light) and can still be strongly absorbed by water (Fig. 5a). The laser induced heating effect was evaluated by the viability of HeLa cells irradiated at different power densities. The cell viability was measured by thiazolyl blue tetazolium bromide
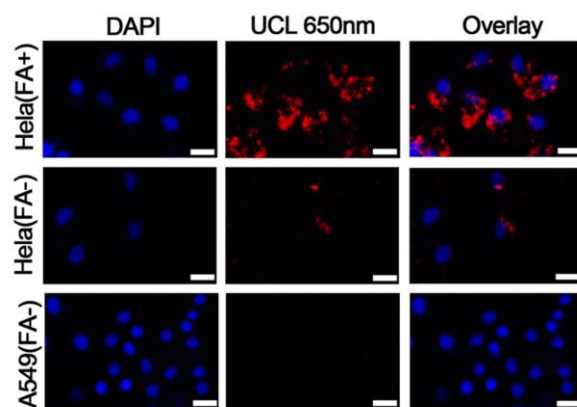

Fig. 6 UCL 650nm images and specificity of UCNPs-RB/FA nanoconstructs under 808 nm laser excitation. Hela cells cultured in folate-free medium (positive, top) and in folate-supplemented medium (negative, middle). The negative control also performed with A549 cells (negative, bottom). From left to right, DAPI-stained cell nuclei, UCL 650nm and Overlay images. All scale bars are 20 µm.

50 (MTT) (Fig. 5b).[20] After 808 nm laser irradiating for 10 minutes, the cell survival rate was 68.54 % at 1.62 W/cm^2 and 95.17 % at 0.67 W/cm^2, respectively. Hence the appropriate power density of irradiation with 808 nm was about 0.67 W/cm^2. By contrast, the cells survival rate was only 51 % at 1.62 W/cm^2 and 65.48 % at
55 0.67 W/cm^2 with 980 nm irradiating for 10 minutes, indicating the much lower overheating effect for cells irradiated with 808 nm. And this low overheating effect of 808 nm irradiation was further confirmed by the morphology changes of pork tissues after irradiating for 10 minutes (Fig. 5c).
60

The red emission of 650 nm of UCNPs could be exploited for bio-imaging purpose, to fulfill photodynamic diagnosis and PDT simultaneously. Nuclei of HeLa cells and human alveolar adenocarcinoma (A549) cells stained in 4, 6-diamidino-2-
65 phenylindole (DAPI) showed blue color (Fig. 6 left). The red emission resulted from the UCNPs-RB upon excitation of 808 nm light. Fig. 6 (top row) shows the bright red emission around the nuclei region indicating UCNPs-RB/FA were entered into the Hela cells. For comparison, control group which was the Hela

cells saturated with UCNPs-RB without linking FA did not have bright UCL (Fig. 6, middle). And A549 cells, poor in expressing folate receptor, were incubated with the same concentration of drugs of UCNPs-RB/FA, also showed obscure red fluorescence (Fig. 6, bottom). More importantly, benefiting from the deep penetration depth of red light emission, UCNPs-RB/FA has the potential in application of image-guided PDT.

In vitro PDT effect of UCNPs was assessed by cell viability. From the absorption spectrum, it was observed that the maximal
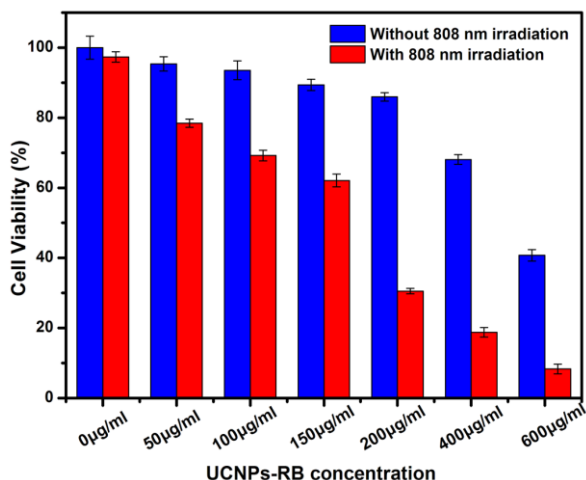

Fig. 7 Viability of Hela cancer cells incubated with different concentration of UCNPs-RB at without (blue histogram) and with (0.67 W/cm^2) (red histogram) 808 nm laser irradiation.

amount of RB per nanoparticle was about 94 (Fig. S14). After incubation with different concentration of UCNPs-RB/FA for 24 h, the Hela cells were irradiated for 10 minutes by 808 nm laser. The cell viability dramatically decreased, while the cells without the irradiation did not show significant change (Fig. 7), indicating that the cell death was dominated by the PDT effect of RB activated by the UCNPs. When the concentration of Nd^{3+}-UCNPs-RB was 200 μg/mL (cells viability was ~85 % without irradiation), Hela cells were killed nearly 44.5 % by PDT. The therapeutic effects nearly reached the level of our previous reports,[15] which performed UCNPs-based PDT with the same photosensitizers of Rose Bengal under irradiation of 980 nm. Different from that, during the process of PDT with 808 nm irradiation, we can irradiate cells or tissues without any interval to avoid the overheating effects. Thus, the Nd^{3+}-UCNPs with critical shell thickness have great potential in bioimaging-guided PDT with 808 nm laser irradiation, may make PDT a more practical method for tumor therapy.

4. Conclusions

In summary, NaYF$_4$:Yb/Ho@NaYF$_4$:Nd@NaYF$_4$ core-shell-shell nanoparticles have been constructed and optimized, aiming at developing luminescence upconversion nanostructures activatable with 808 nm light for FRET-based applications, especially for PDT. Trade-off between robust upconversion emission and efficient transfer of excitation energy from the nanoparticles to photosensitizers was reached. Inert layer was particular effective to offset the loss due to shortening the active layer. Proof of concept test was performed for cell imaging and PDT simultaneously of Hela cells under excitation of 808 nm, where minimization of overheating effect was confirmed from the comparison with popular excitation of 980 nm.

Notes and references

^{a} State Key Laboratory of Luminescence and Applications, Changchun Institute of Optics, Fine Mechanics and Physics, Chinese Academy of Sciences, Changchun 130033, China.
^{b} Graduate University of the Chinese Academy of Sciences, Beijing 100049, China.
^{c} Department of Basic Medicine, Gerontology Department of First Bethune Hospital, University of Jilin, Changchun 130021, China.
^{d} Van't Hoff Institute for Molecular Sciences, University of Amsterdam, Science Park 904, 1098 XH Amsterdam, The Netherlands.
$^+$These authors contributed equally to this work.
* Corresponding author:
E-mail: xgkong14@ciomp.ac.cn; h.zhang@uva.nl
†Electronic Supplementary Information (ESI) available: TEM images, XRD and NIR emission spectra of UCNPs.

1. J. Wang, R. Deng, M. A. MacDonald, B. Chen, J. Yuan, F. Wang, D. Chi, T. S. A. Hor, P. Zhang and G. Liu, *Nat. Mater.* , 2014, **13**, 157-162.
2. D. J. Gargas, E. M. Chan, A. D. Ostrowski, S. Aloni, M. V.P. Altoe, E. S. Barnard, B. Sanii, J. J. Urban, D. J. Milliron and B. E. Cohen, *Nat. Nanotechnol.* , 2014, **9**, 300-305.
3. F. Wang and X. Liu, *Acc. Chem. Res.* , 2014, **47**, 1378-1385.
4. W.-P. Qin, Z.-Y. Liu, C.-N. Sin, C.-F. Wu, G.-S. Qin, Z. Chen and K.-Z. Zheng, *Light: Science & Applications*, 2014, **3**, e193.
5. W. Zou, C. Visser, J. A. Maduro, M. S. Pshenichnikov and J. C. Hummelen, *Nat. Photonics* 2012, **6**, 560-564.
6. X. Xie and X. Liu, *Nat. Mater.* , 2012, **11**, 842-843.
7. G. Chen, J. Shen, T. Y. Ohulchanskyy, N. J. Patel, A. Kutikov, Z. Li, J. Song, R. K. Pandey, H. Ågren and P. N. Prasad, *ACS nano*, 2012, **6**, 8280-8287.
8. L. Zhou, Z. Li, Z. Liu, M. Yin, J. Ren and X. Qu, *Nanoscale*, 2014, **6**, 1445-1452.
9. Y. Liu, D. Tu, H. Zhu, E. Ma and X. Chen, *Nanoscale*, 2013, **5**, 1369-1384.
10. Y. Zhou, S.-T. Han, X. Chen, F. Wang, Y.-B. Tang and V. Roy, *Nat. Commun.*, 2014, **5**. doi:10.1038/ncomms5720.
11. T. Wu, M. Barker, K. M. Arafeh, J.-C. Boyer, C.-J. Carling and N. R. Branda, *Angew. Chem., Int. Ed.*,, 2013, **52**, 11106-11109.
12. D. Tu, L. Liu, Q. Ju, Y. Liu, H. Zhu, R. Li and X. Chen, *Angew. Chem., Int. Ed.*,, 2011, **50**, 6306-6310.
13. N. M. Idris, M. K. Gnanasammandhan, J. Zhang, P. C. Ho, R. Mahendran and Y. Zhang, *Nat. Med.* , 2012, **18**, 1580-1585.
14. Q. Zhan, J. Qian, H. Liang, G. Somesfalean, D. Wang, S. He, Z. Zhang and S. Andersson-Engels, *ACS nano*, 2011, **5**, 3744-3757.
15. J. Shen, G. Chen, A. M. Vu, W. Fan, O. S. Bilsel, C. C. Chang and G. Han, *Adv. Opt. Mater.*, 2013. **1**, 644-650.
16. Y.-F. Wang, G.-Y. Liu, L.-D. Sun, J.-W. Xiao, J.-C. Zhou and C.-H. Yan, *ACS nano*, 2013, **7**, 7200-7206.
17. X. Xie, N. Gao, R. Deng, Q. Sun, Q. Xu and X. Liu, *J. Am. Chem. Soc.* , 2013, **135**, 12608-12611.

18. H. Wen, H. Zhu, X. Chen, T. F. Hung, B. Wang, G. Zhu, S. F. Yu and F. Wang, *Angew. Chem., Int. Ed.*, 2013, **52**, 13419-13423.

19. Y. Zhong, G. Tian, Z. Gu, Y. Yang, L. Gu, Y. Zhao, Y. Ma and J. Yao, *Adv. Mater.* , 2013, **26**, 2831-2837.

5 20. Y. Wang, K. Liu, X. Liu, K. Dohnalová T. Gregorkiewicz, X. Kong, M. C. Aalders, W. J. Buma and H. Zhang, J. Phys. Chem. Lett., 2011, **2**, 2083-2088.

21. N. J. Johnson, A. Korinek, C. Dong and F. C. van Veggel, *J. Am. Chem. Soc.* , 2012, **134**, 11068-11071.

10 22. G. H. Dieke and B. Pandey, *J. Chem. Phys.*, 1964, **41**, 1952-1969.

23. K. Liu, X. Liu, Q. Zeng, Y. Zhang, L. Tu, T. Liu, X. Kong, Y. Wang, F. Cao and S. A. Lambrechts, *ACS nano*, 2012, **6**, 4054-4062.

24. J. J. Lamberts, D. R. Schumacher and D. Neckers, *J. Am. Chem. Soc.* , 1984, **106**, 5879-5883.

15 25. P. B. Merkel and D. R. Kearns, *J. Am. Chem. Soc.* , 1975, **97**, 462-463.

26. F. Wang, J. Wang and X. Liu, *Angew. Chem., Int. Ed.,* 2010, **49**, 7456-7460.

27. J. R. Lakowicz, *Principles of fluorescence spectroscopy*, Springer, 20 2007.

28. D. Gerlier and N. Thomasset, *J. Immunol. Methods.*, 1986, **94**, 57-63.